Proceedings of 20th International Congress on Acoustics, ICA 2010

23-27 August 2010, Sydney, Australia

Prediction by the finite-difference time-domain method for vibroacoustic problems

Masahiro Toyoda (1) and Daiji Takahashi (2)

(1) Kyoto University Pioneering Research Unit, B104, Kyoto University Katsura, Nishikyo-ku, Kyoto, 615-8530, Japan
(2) Dept. of Architecture and Architectural Eng., Graduate School of Eng., Kyoto University, C1-4-385, Kyoto University Katsura, Nishikyo-ku, Kyoto, 615-8540, Japan

PACS: 43.40.At, 43.55Ka

ABSTRACT

The finite-difference time-domain method considering longitudinal and shear waves and two types of damping terms has been proposed as a prediction method for structure-borne sound. In the method, both solids and fluids are assumed to be governed by a unique set of motion equations and viscoelastic constitutive equations using averaged material parameters. Herein the formulation of the method for inhomogeneous anisotropic media is presented and some numerical examples are shown. The comparison between predicted and measured data of floor impact noise in a two-story concrete building is first introduced from the viewpoints of energy decay and frequency characteristics. Next, to investigate the accuracy of the prediction method, the numerical results for a simple vibroacoustic system of a circular plate clamped in a duct are compared with analytical ones obtained by the thin-plate theory. In the comparison, discrepancies in eigenfrequency can be observed because the considered plate is rather thick. However the predicted eigenfrequencies *in vacuo* well correspond with those derived from the thick-plate theory. Last, propagation of waves in a wooden block and the radiated sound are calculated and the numerical results are compared with the measured ones. Although the material parameters need to be identified by use of the measured data, the calculated results can be in good agreement with the measured ones.

INTRODUCTION

The finite-difference time-domain (FDTD) method was originally developed in the field of electromagnetics [1], and it has been investigated for a long time [2-4]. Recently, this method has been widely studied in various acoustical fields, including ultrasonics [5], underwater sound [6], etc.. In architectural acoustics, this method has been applied to hall acoustics [7-9] and traffic noise problems [10], and is currently attracting a great deal of attention as a prediction method and a visualization tool for sound fields. As for vibroacoustic problems, the insulation performance of double-leaf windows has been investigated using thin plate theory with the acoustical FDTD method [11].

The authors investigated the possibility of employing the vibroacoustic FDTD method, which considers longitudinal and shear waves as well as two type of damping, to predict the architectural structure-borne sound [12]. In the method, both solids and fluids are assumed to be governed by a unique set of motion equations and viscoelastic constitutive equations using averaged material parameters. Consequently, the vibroacoustic problems can be reduced to inhomogeneous problems in the method. However, the formulation is limited to isotropic media. Herein, as a further study of the method, the formulation for inhomogeneous anisotropic media is presented and some numerical examples are also shown. Although there have been some studies on the finite-difference method for anisotropic media [13, 14], damping terms have not been considered.

First, the comparisons between predicted and measured data of floor impact noise in a two-story concrete building are introduced from the viewpoints of energy decay and frequency characteristics [12]. Next, considering a simple vibroacoustic system of a circular plate clamped in a duct, the numerical results obtained by the FDTD method are compared with analytical ones derived from the thin-plate theory to investigate the accuracy of the prediction method. Last, propagation of waves in a wooden block and the radiated sound are calculated and the numerical results are compared with measured ones.

FORMULATION

Basic equations

Considering the condition of small deformation, adiabatic transition, and athermic media, a unique set of motion equations and viscoelastic constitutive equations with two types of damping terms is expressed in tensor notation as

$$\rho \frac{\partial v_i}{\partial t} + \zeta v_i = \frac{\partial T_{ij}}{\partial a_j}, \tag{1}$$

$$T_{ij} = c_{ijkl}\varepsilon_{kl} + \xi_{ijkl}e_{kl}, \tag{2}$$

where ρ is the density, v is the velocity vector, t is time, ζ is a constant to describe the damping force proportional only to the velocity and is also used to model the wave propagation

in porous materials [15], T is the stress tensor, a(=[x, y, z]) is the position vector, c is the stiffness tensor, ε is the strain tensor, ξ is the viscosity tensor, which describes the damping force proportional to the second-order space derivative of the velocity, and e(=$\partial\varepsilon/\partial t$) is the strain velocity tensor. It should be noted that a combination of two types of damping terms ζ and ξ yields similar characteristics to the Rayleigh damping. Considering the reciprocity of stiffness and viscosity, the stiffness tensor c and the viscosity tensor ξ can be abbreviated to the matrix forms which respectively have 21 independent constants. In addition, if orthotropic media are considered, the constants can be reduced to 9 independent ones. In this case, the relationship between c and Young's moduli E, shear moduli G, and Poisson's ratios υ can be given by

$$\mathbf{c} = \mathbf{s}^{-1}, \tag{3}$$

$$\frac{\upsilon_{xy}}{E_x} = \frac{\upsilon_{yx}}{E_y}, \ \frac{\upsilon_{yz}}{E_y} = \frac{\upsilon_{zy}}{E_z}, \ \frac{\upsilon_{zx}}{E_z} = \frac{\upsilon_{xz}}{E_x}, \tag{4}$$

$$\mathbf{s} = \begin{bmatrix} \frac{1}{E_x} & -\frac{\upsilon_{xy}}{E_x} & -\frac{\upsilon_{xz}}{E_x} & 0 & 0 & 0 \\ -\frac{\upsilon_{yx}}{E_y} & \frac{1}{E_y} & -\frac{\upsilon_{yz}}{E_y} & 0 & 0 & 0 \\ -\frac{\upsilon_{zx}}{E_z} & -\frac{\upsilon_{zy}}{E_z} & \frac{1}{E_z} & 0 & 0 & 0 \\ 0 & 0 & 0 & \frac{1}{G_{xy}} & 0 & 0 \\ 0 & 0 & 0 & 0 & \frac{1}{G_{yz}} & 0 \\ 0 & 0 & 0 & 0 & 0 & \frac{1}{G_{zx}} \end{bmatrix}, \tag{5}$$

where **c** is the stiffness matrix and **s** is the compliance matrix. For a fluid, the bulk modulus κ and zero should be substituted for c_{11}=c_{22}=c_{33}=c_{12}=c_{13}=c_{23} and c_{44}=c_{55}=c_{66}, respectively. In this case, Eq. (2) means the constitutive equation of a Newtonian fluid. The linearized Navier-Stokes equation, where a convection term and a volumetric force are neglected, can be derived by substituting Eq. (2) into Eq. (1). The sound pressure can be obtained by calculating $-\kappa\nabla\mathbf{u}$, where **u** means the displacement vector. In this study, perfectly matched layers (PMLs) [16, 17] are employed as absorption layers located outside the target region. The PML medium is a non-physical material, which has the same characteristic impedance as the adjacent medium and also attenuates wave propagation. Therefore, waves that propagate in the PML medium do not generally satisfy the classical wave equation. However, existing materials can be expressed in the same forms as the PML medium by selecting the appropriate constants. Accordingly, Eqs. (1) and (2) can be rewritten as

$$\rho\frac{\partial v_{x,x}}{\partial t} + \zeta_{x,x}v_{x,x} = \frac{\partial \sigma_{xx}}{\partial x}, \tag{6}$$

$$\rho\frac{\partial v_{x,y}}{\partial t} + \zeta_{x,y}v_{x,y} = \frac{\partial \tau_{xy}}{\partial y}, \tag{7}$$

$$\rho\frac{\partial v_{x,z}}{\partial t} + \zeta_{x,z}v_{x,z} = \frac{\partial \tau_{zx}}{\partial z}, \tag{8}$$

$$\rho\frac{\partial v_{y,x}}{\partial t} + \zeta_{y,x}v_{y,x} = \frac{\partial \tau_{xy}}{\partial x}, \tag{9}$$

$$\rho\frac{\partial v_{y,y}}{\partial t} + \zeta_{y,y}v_{y,y} = \frac{\partial \sigma_{yy}}{\partial y}, \tag{10}$$

$$\rho\frac{\partial v_{y,z}}{\partial t} + \zeta_{y,z}v_{y,z} = \frac{\partial \tau_{yz}}{\partial z}, \tag{11}$$

$$\rho\frac{\partial v_{z,x}}{\partial t} + \zeta_{z,x}v_{z,x} = \frac{\partial \tau_{zx}}{\partial x}, \tag{12}$$

$$\rho\frac{\partial v_{z,y}}{\partial t} + \zeta_{z,y}v_{z,y} = \frac{\partial \tau_{yz}}{\partial y}, \tag{10}$$

$$\rho\frac{\partial v_{z,z}}{\partial t} + \zeta_{z,z}v_{z,z} = \frac{\partial \sigma_{zz}}{\partial z}, \tag{13}$$

$$\frac{\partial \sigma_{xx,x}}{\partial t} + \zeta'_x\sigma_{xx,x} = c_{11}\frac{\partial v_x}{\partial x} + \xi_{11}\frac{\partial^2 v_x}{\partial x\partial t}, \tag{14}$$

$$\frac{\partial \sigma_{xx,y}}{\partial t} + \zeta'_y\sigma_{xx,y} = c_{12}\frac{\partial v_y}{\partial y} + \xi_{12}\frac{\partial^2 v_y}{\partial y\partial t}, \tag{15}$$

$$\frac{\partial \sigma_{xx,z}}{\partial t} + \zeta'_z\sigma_{xx,z} = c_{13}\frac{\partial v_z}{\partial z} + \xi_{13}\frac{\partial^2 v_z}{\partial z\partial t}, \tag{16}$$

$$\frac{\partial \sigma_{yy,x}}{\partial t} + \zeta'_x\sigma_{yy,x} = c_{12}\frac{\partial v_x}{\partial x} + \xi_{12}\frac{\partial^2 v_x}{\partial x\partial t}, \tag{17}$$

$$\frac{\partial \sigma_{yy,y}}{\partial t} + \zeta'_y\sigma_{yy,y} = c_{22}\frac{\partial v_y}{\partial y} + \xi_{22}\frac{\partial^2 v_y}{\partial y\partial t}, \tag{18}$$

$$\frac{\partial \sigma_{yy,z}}{\partial t} + \zeta'_z\sigma_{yy,z} = c_{23}\frac{\partial v_z}{\partial z} + \xi_{23}\frac{\partial^2 v_z}{\partial z\partial t}, \tag{19}$$

$$\frac{\partial \sigma_{zz,x}}{\partial t} + \zeta'_x\sigma_{zz,x} = c_{13}\frac{\partial v_x}{\partial x} + \xi_{13}\frac{\partial^2 v_x}{\partial x\partial t}, \tag{20}$$

$$\frac{\partial \sigma_{zz,y}}{\partial t} + \zeta'_y\sigma_{zz,y} = c_{23}\frac{\partial v_y}{\partial y} + \xi_{23}\frac{\partial^2 v_y}{\partial y\partial t}, \tag{21}$$

$$\frac{\partial \sigma_{zz,z}}{\partial t} + \zeta'_z\sigma_{zz,z} = c_{33}\frac{\partial v_z}{\partial z} + \xi_{33}\frac{\partial^2 v_z}{\partial z\partial t}, \tag{22}$$

$$\frac{\partial \tau_{xy,x}}{\partial t} + \zeta'_x\tau_{xy,x} = c_{44}\frac{\partial v_y}{\partial x} + \xi_{44}\frac{\partial^2 v_y}{\partial x\partial t}, \tag{23}$$

$$\frac{\partial \tau_{xy,y}}{\partial t} + \zeta'_y\tau_{xy,y} = c_{44}\frac{\partial v_x}{\partial y} + \xi_{44}\frac{\partial^2 v_x}{\partial y\partial t}, \tag{24}$$

$$\frac{\partial \tau_{yz,y}}{\partial t} + \zeta'_y\tau_{yz,y} = c_{55}\frac{\partial v_z}{\partial y} + \xi_{55}\frac{\partial^2 v_z}{\partial y\partial t}, \tag{25}$$

$$\frac{\partial \tau_{yz,z}}{\partial t} + \zeta'_z\tau_{yz,z} = c_{55}\frac{\partial v_y}{\partial z} + \xi_{55}\frac{\partial^2 v_y}{\partial z\partial t}, \tag{26}$$

$$\frac{\partial \tau_{zx,z}}{\partial t} + \zeta'_z\tau_{zx,z} = c_{66}\frac{\partial v_x}{\partial z} + \xi_{66}\frac{\partial^2 v_x}{\partial z\partial t}, \tag{27}$$

$$\frac{\partial \tau_{zx,x}}{\partial t} + \zeta'_x\tau_{zx,x} = c_{66}\frac{\partial v_z}{\partial x} + \xi_{66}\frac{\partial^2 v_z}{\partial x\partial t}, \tag{28}$$

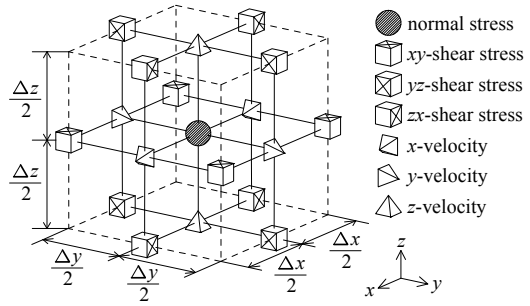

Figure 1. Three-dimensional staggered grid system.

where $v_x=v_{x,x}+v_{x,y}+v_{x,z}=v_1$ is the x-directional velocity, $v_y=v_{y,x}+v_{y,y}+v_{y,z}=v_2$ is the y-directional velocity, $v_z=v_{z,x}+v_{z,y}+v_{z,z}=v_3$ is the z-directional velocity, $\sigma_{xx}=\sigma_{xx,x}+\sigma_{xx,y}+\sigma_{xx,z}=T_{11}$ is the x-directional normal stress, $\sigma_{yy}=\sigma_{yy,x}+\sigma_{yy,y}+\sigma_{yy,z}=T_{22}$ is the y-directional normal stress, $\sigma_{zz}=\sigma_{zz,x}+\sigma_{zz,y}+\sigma_{zz,z}=T_{33}$ is the z-directional normal stress, $\tau_{xy}=\tau_{xy,x}+\tau_{xy,y}=T_{12}=T_{21}$ is the shear stress defined in the xy-plane, $\tau_{yz}=\tau_{yz,y}+\tau_{yz,z}=T_{23}=T_{32}$ is the shear stress defined in the yz-plane, and $\tau_{zx}=\tau_{zx,z}+\tau_{zx,x}=T_{31}=T_{13}$ is the shear stress defined in the zx-plane. $\zeta_{d,x}=\zeta_{d,y}=\zeta_{d,z}(=\zeta_d)$ (d=x, y, z) in parts other than the PMLs and $\zeta_{x,d}=\zeta_{y,d}=\zeta_{z,d}(=\zeta'_d)$ in the PMLs. ζ'_d are constants used for impedance matching in the PMLs. In parts other than the PMLs, the constants must be zero.

Averaging of material parameters

Reference points for the stress and velocity are arranged on the staggered-grid system shown in Fig. 1. Δx, Δy, and Δz are the spatial intervals between the reference points of normal stress for the x, y, and z directions and their point locations are expressed by i, j, and k, respectively. Although the spatial intervals between the reference points of shear stress and velocity are identical to those of normal stress, their point locations should be properly shifted according to the staggered-grid system. Hence, for example, the point locations of xy-shear stress are expressed by i+0.5, j+0.5, and k, and those of x-velocity are expressed by i+0.5, j, and k. Δt is the time interval for the calculation, and the elapsed-time counter is given by superscript n for normal and shear stresses and n+0.5 for velocities.

The target region of a vibroacoustic problem can be considered to be filled with an inhomogeneous anisotropic material which is governed by Eqs. (1) and (2). Herein, all material parameters are defined at the reference points of normal stress and the mean values are used at the reference points of velocity and shear stress [18-22]. At the reference points of velocity, arithmetic averages are employed, for example:

$$\overline{\rho}(i+0.5,j,k)=\frac{\rho(i,j,k)+\rho(i+1,j,k)}{2}. \tag{29}$$

At the reference points of shear stress, harmonic averages are employed, for example:

$$\overline{\overline{c_{44}}}(i+0.5,j+0.5,k)=4\left\{\frac{1}{c_{44}(i,j,k)}+\frac{1}{c_{44}(i+1,j,k)}+\frac{1}{c_{44}(i,j+1,k)}+\frac{1}{c_{44}(i+1,j+1,k)}\right\}^{-1}. \tag{30}$$

The damping constants are also given by their arithmetic averages at velocity points and by their harmonic averages at shear-stress points.

Boundary conditions

Multiple boundary conditions should be considered: a fixed boundary, a free boundary, and an absorption boundary. As mentioned in the preceding section, the PMLs are employed as the absorption layers in this study. Hence, the following is devoted to a fixed boundary and a free boundary. Herein both the fixed and free boundaries are defined at the plane, which includes the reference points of velocity and shear stress.

On a fixed boundary, velocities in all directions must be zero. This condition can be directly satisfied at the reference points of velocity located on the boundary. However, because the reference points of the parallel-directional velocity to the boundary surface are not defined just on the boundary, virtual reference points are assumed outside the boundary, and their values are determined so that the mean velocities on the boundary are zero. For example under the condition where the plane i+0.5=I+0.5 is assumed to be a fixed boundary,

$$\begin{cases} v_x(I+0.5,j,k)=0 \\ v_y(I,j\pm0.5,k)+v_y(I+1,j\pm0.5,k)=0 \\ v_z(I,j,k\pm0.5)+v_y(I+1,j,k\pm0.5)=0 \end{cases}. \tag{31}$$

On a free boundary, the normal stress to the boundary surface and shear stresses defined in normal planes to the boundary surface should be zero. Similar to the case of a fixed boundary, the reference points of normal stress, which should be zero, are not arranged on the boundary. Therefore, virtual reference points are assumed outside the boundary, and their values are determined so that the mean normal stresses just on the boundary are zero. For example under the condition where the plane i+0.5=I+0.5 is assumed to be a free boundary,

$$\begin{cases} \tau_{xy}(I+0.5,j\pm0.5,k)=\tau_{zx}(I+0.5,j,k\pm0.5)=0 \\ \sigma_{xx}(I,j,k)+\sigma_{xx}(I+1,j,k)=0 \end{cases}. \tag{32}$$

Discretization

For example, Eq. (6) is discretized with a central difference as:

$$\begin{aligned} &\overline{\rho}(i+0.5,j,k)\frac{v_{x,x}^{n+0.5}(i+0.5,j,k)-v_{x,x}^{n-0.5}(i+0.5,j,k)}{\Delta t} \\ &+\overline{\overline{\varsigma_{x,x}}}(i+0.5,j,k)\frac{v_{x,x}^{n+0.5}(i+0.5,j,k)+v_{x,x}^{n-0.5}(i+0.5,j,k)}{2} \\ &\approx\frac{\sigma_{xx}^{n}(i+1,j,k)-\sigma_{xx}^{n}(i,j,k)}{\Delta x} \end{aligned} \tag{33}$$

Eq. (14) is discretized with a backward difference for time derivation of the viscosity term and central difference for other terms as:

$$\begin{aligned} &\frac{\sigma_{xx,x}^{n+1}(i,j,k)-\sigma_{xx,x}^{n}(i,j,k)}{\Delta t} \\ &+\zeta'_x(i,j,k)\frac{\sigma_{xx,x}^{n+1}(i,j,k)+\sigma_{xx,x}^{n}(i,j,k)}{2} \\ &\approx\left\{c_{11}(i,j,k)+\frac{\xi_{11}(i,j,k)}{\Delta t}\right\}\times \\ &\frac{v_x^{n+0.5}(i+0.5,j,k)-v_x^{n+0.5}(i-0.5,j,k)}{\Delta x} \\ &-\frac{\xi_{11}(i,j,k)}{\Delta t}\frac{v_x^{n-0.5}(i+0.5,j,k)-v_x^{n-0.5}(i-0.5,j,k)}{\Delta x} \end{aligned} \tag{34}$$

Transforming these discretized equations, updating formulas for $v_{x,x}{}^{n+0.5}(i+0.5, j, k)$ and $\sigma_{xx,x}{}^{n+1}(i, j, k)$ can be obtained. Updating formulas for other variables can be obtained by a similar procedure.

Stability condition

This section is devoted to the stability conditions in the case of discretization as described in the preceding section. An arbitrary wave can be expressed as a superposition of plane waves. Therefore, the stability conditions for a plane wave of an arbitrary propagation angle are derived here [3]. To consider the plane wave, velocities and stresses are, for example, expressed as

$$v_x^{n+0.5}\left(i+0.5, j, k\right) = v_{x0}^{n+0.5} e^{\mathrm{i}\left\{k_x(i+0.5)\Delta x + k_y j\Delta y + k_z k\Delta z\right\}}, \tag{35}$$

$$\sigma_{xx}^{n}\left(i, j, k\right) = \sigma_{xx0}^{n} e^{\mathrm{i}\left\{k_x i\Delta x + k_y j\Delta y + k_z k\Delta z\right\}}, \tag{36}$$

$$\tau_{xy}^{n}\left(i+0.5, j+0.5, k\right) = \tau_{xy0}^{n} e^{\mathrm{i}\left\{k_x(i+0.5)\Delta x + k_y(j+0.5)\Delta y + k_z k\Delta z\right\}}, \tag{37}$$

where i is the imaginary unit, k_x, k_y, and k_z are x, y, and z-directional wave number, respectively. Substituting Eqs. (35)-(37), etc. into Eqs. (6)-(28) with ζ'_d=0 yields a homogeneous state-difference equation expressed by

$$\mathbf{x}^{n+1} = \mathbf{A}\mathbf{x}^{n}, \tag{38}$$

where

$$\left[\mathbf{x}^{n}\right]^{*} = \left[v_{x0}^{n-0.5} \quad v_{y0}^{n-0.5} \quad v_{z0}^{n-0.5} \quad \sigma_{xx0}^{n} \quad \sigma_{yy0}^{n} \quad \sigma_{zz0}^{n} \quad \tau_{xy0}^{n} \quad \tau_{yz0}^{n} \quad \tau_{zx0}^{n}\right], \tag{39}$$

$$\mathbf{A} = \begin{bmatrix}
r_x & 0 & 0 & R_x s_x & 0 & 0 \\
0 & r_y & 0 & 0 & R_y s_y & 0 \\
0 & 0 & r_z & 0 & 0 & R_z s_z \\
b_{11x}s_x & b_{12y}s_y & b_{13z}s_z & 1-B_{11x}s_x^2 & -B_{12y}s_y^2 & -B_{13z}s_z^2 \\
b_{12x}s_x & b_{22y}s_y & b_{23z}s_z & -B_{12x}s_x^2 & 1-B_{22y}s_y^2 & -B_{23z}s_z^2 \\
b_{13x}s_x & b_{23y}s_y & b_{33z}s_z & -B_{13x}s_x^2 & -B_{23y}s_y^2 & 1-B_{33z}s_z^2 \\
b_{44x}s_y & b_{44y}s_x & 0 & -B_{44x}s_x s_y & -B_{44y}s_x s_y & 0 \\
0 & b_{55y}s_z & b_{55z}s_y & 0 & -B_{55y}s_y s_z & -B_{55z}s_y s_z \\
b_{66x}s_z & 0 & b_{66z}s_x & -B_{66x}s_z s_x & 0 & -B_{66z}s_z s_x
\end{bmatrix}$$

$$\begin{bmatrix}
R_x s_y & 0 & R_x s_z \\
R_y s_x & R_y s_z & 0 \\
0 & R_z s_y & R_z s_x \\
-\left(B_{11x}+B_{12y}\right)s_x s_y & -\left(B_{12y}+B_{13z}\right)s_y s_z & -\left(B_{13z}+B_{11x}\right)s_z s_x \\
-\left(B_{12x}+B_{22y}\right)s_x s_y & -\left(B_{22y}+B_{23z}\right)s_y s_z & -\left(B_{23z}+B_{12x}\right)s_z s_x \\
-\left(B_{13x}+B_{23y}\right)s_x s_y & -\left(B_{23y}+B_{33z}\right)s_y s_z & -\left(B_{33z}+B_{13x}\right)s_z s_x \\
1-B_{44y}s_x^2-B_{44x}s_y^2 & -B_{44y}s_z s_x & -B_{44x}s_y s_z \\
-B_{55y}s_z s_x & 1-B_{55z}s_y^2-B_{55y}s_z^2 & -B_{55z}s_x s_y \\
-B_{66x}s_y s_z & -B_{66z}s_x s_y & 1-B_{66x}s_z^2-B_{66z}s_x^2
\end{bmatrix} \tag{40}$$

$$\theta_d = \frac{\Delta t}{2\rho}\zeta_d, \tag{41}$$

$$r_d = \frac{1-\theta_d}{1+\theta_d}, \tag{42}$$

$$R_d = \frac{\mathrm{i}\Delta t}{\rho\left(1+\theta_d\right)}, \tag{43}$$

$$b_{\alpha d} = \mathrm{i}\Delta t\left\{\frac{c_\alpha\left(1-\theta_d\right)-2\xi_\alpha\theta_d}{1+\theta_d}\right\}, \tag{44}$$

$$B_{\alpha d} = \frac{c_\alpha\Delta t^2-\xi_\alpha\Delta t}{\rho\left(1+\theta_d\right)}, \tag{45}$$

$$s_d = \frac{2\sin\left(k_d\dfrac{\Delta d}{2}\right)}{\Delta d}, \tag{46}$$

where the asterisk denotes the transpose, α=11, 22, 33, 12, 13, 23, 44, 55, 66, and d=x, y, z. To obtain stable solutions from Eq. (38), all eigenvalues must be one or less for an arbitrary propagation angle, i.e., for an arbitrary coupling of k_x, k_y, and k_z. Therefore, assigning s_x, s_y, and s_z to their maximum values of $2/\Delta x$, $2/\Delta y$, and $2/\Delta z$ respectively, should enable Δt to be determined so that all eigenvalues of the matrix **A** are less than or equal to one.

Initial condition and excitation

In this paper, all initial values of velocities and stresses are set to zero. An input excitation is assumed to be a point force $F(t)$. In this case, $F(n\Delta t)/\Delta S$ should be added to the normal stress in the excitation direction, which belongs to the spatial difference term in the updating formula of velocity. ΔS is the unit area normal to the excitation direction, for example, $\Delta S = \Delta y\Delta z$ for x-directional excitation.

NUMERICAL EXAMPLES

Floor impact noise

In this section, the comparisons between the predicted and measured data of floor impact noise are introduced [12]. Figure 2 shows the cross section and the plan of the two-story concrete building to be calculated. Two excitation points (Exc. 1 and 2), which are denoted in the figure, are considered. Figure 3 shows a picture of the experiment. In the calculations, the excitation waves are assumed to be Gaussian

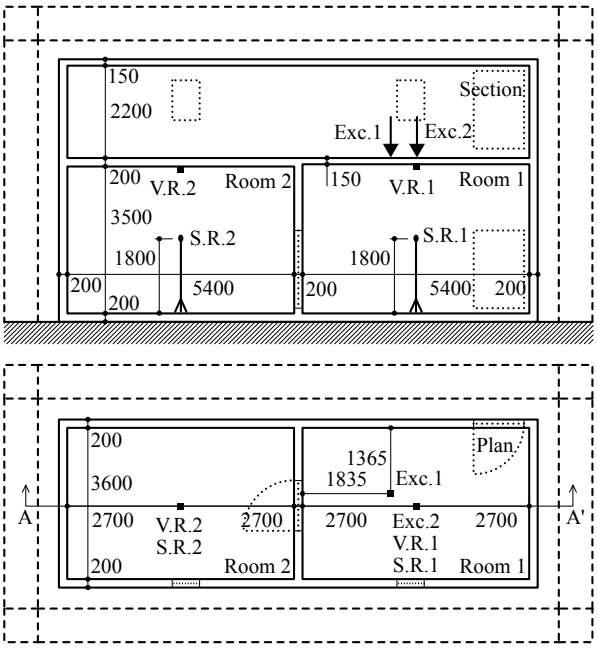

Figure 2. Section and plan of the two-story concrete building.

Figure 3. Picture of the experiment.

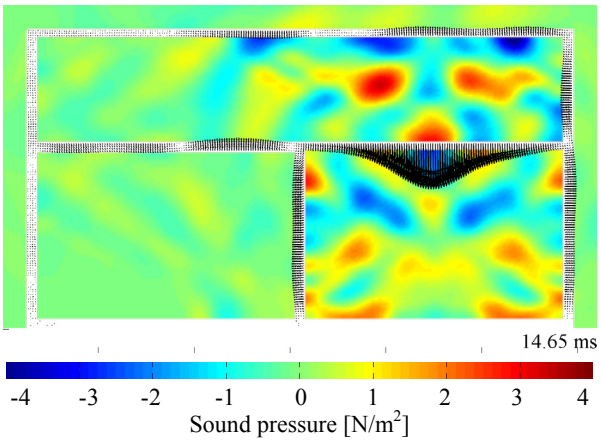

Figure 4. Distribution of displacements and sound pressures.

pulses in which the coefficients are determined so that the waveforms are similar to the measured force data of the impulse hummer used in the measurements. In each room, two vibration receivers (V. R. 1 and 2) are located at the centre of the ceiling, and two sound receivers (S. R. 1 and 2) are at the centre. In the measurements, acceleration pickups and microphones are located at these points. Velocities in the normal direction are calculated by integrating measured acceleration values and sound pressures are measured at a sampling frequency of 44100 Hz. As for the boundary conditions, the ground surface is assumed to be a fixed boundary, and in the Fig. 2, areas enclosed with broken lines are assumed to be PMLs. All the building frames are assumed to be isotropic concrete with a density of 2400 kg/m^3, Young's modulus of 2.4×10^{10} N/m^2, and Poisson's ratio of 0.2. All rooms as well as outdoors are assumed to be filled with air with a density of 1.205 kg/m^3 ($=\rho_0$) and a bulk modulus of 1.422×10^5 N/m^2. The maximum target frequency in the calculations is set to 500 Hz. Allowing for this, spatial intervals $\Delta x=\Delta y=\Delta z$ are set to 50 mm. Viscosity coefficients for air are set as $\xi_{11}=\xi_{22}=\xi_{33}=3.6 \times 10^{-5}$, $\xi_{12}=\xi_{13}=\xi_{23}=0$, and $\zeta_{11}=\zeta_{22}=\zeta_{33}=1.8 \times 10^{-5}$ Ns/m^2, while those for concrete are assumed to be proportional to the initial stiffness, i.e., $\boldsymbol{\zeta}=\eta\mathbf{c}/\omega_0$ where $\boldsymbol{\zeta}$ is viscosity matrix, η is loss factor and ω_0 is the first-order natural angular frequency of the building. The assumed loss factor of the concrete is 0.005, and first-order natural angular frequency is set at $2\pi \times 32$ rad/s. constants ζ_d is set as $\zeta_x=\zeta_y=\zeta_z=2.5 \times 10^4$ Ns/m^4 for concrete and $\zeta_x=\zeta_y=\zeta_z=5$ Ns/m^4 for air. Allowing for these assumptions and the stability condition, the time interval is determined to 1 μs.

Although the predictions and the measurements were performed for two of excitation points, only the comparisons for Exc. 2 are shown here because the comparisons for Exc. 1 have been already presented [12]. Figure 4 shows an example

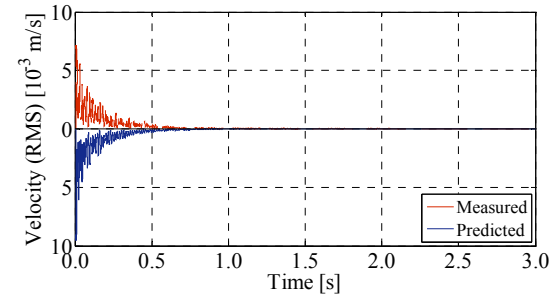

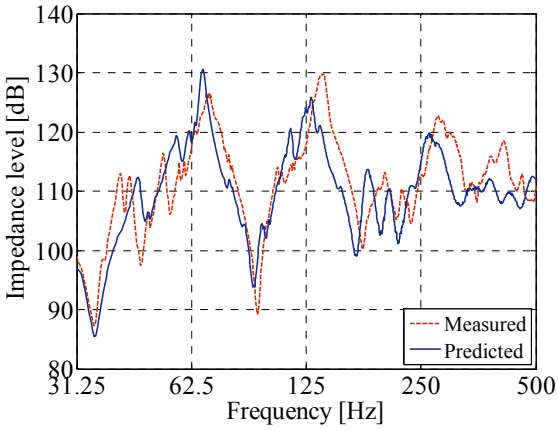

Figure 5. Predicted and measured data at V. R. 1.

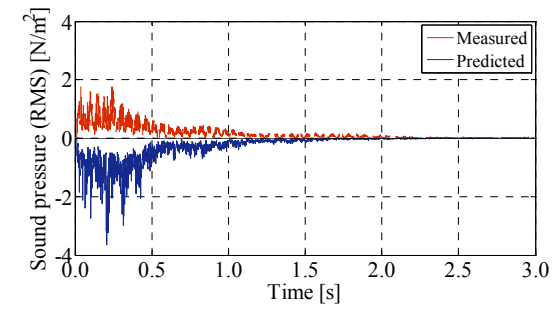

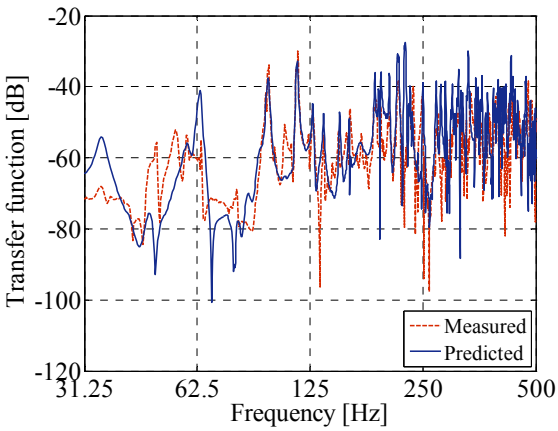

Figure 6. Predicted and measured data at S. R. 1.

of the visualized field of displacement and sound pressure at section A-A' shown in Fig. 2. Displacements are expressed with black arrows at the reference points of the concrete, whereas sound pressures at the reference points of air are expressed with the colors shown in the color bar. To aid in the understanding, the displacements in the figure are multiplied by 80000. Figures 5 and 6 show the examples of echo diagrams (RMS) at V. R. 1 and S. R. 1, the impedance levels

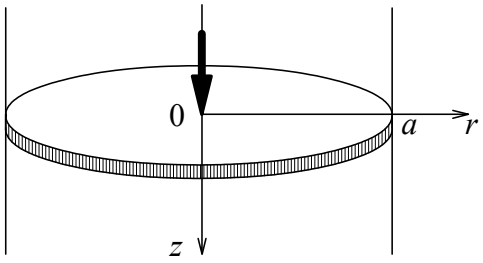

Figure 7. Configuration of a circular plate clamped in a duct.

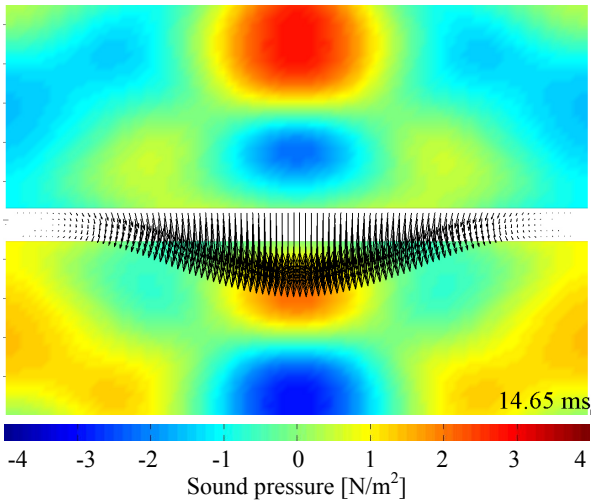

Figure 8. Distribution of displacements and sound pressures.

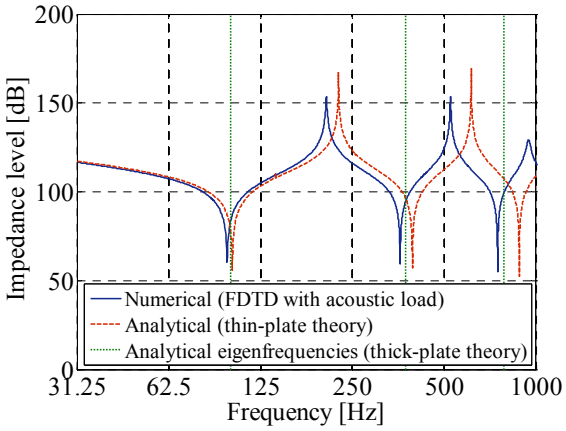

Figure 9. Numerical and analytical results of the impedance.

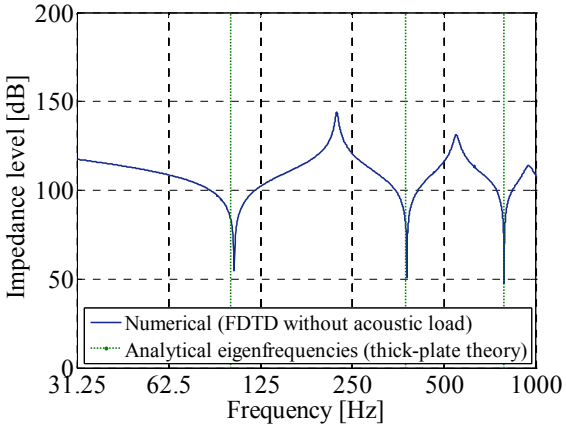

Figure 10. Numerical and analytical results of the impedance.

at V. R. 1, and the transfer functions by a unit excitation at S. R. 1. Although some discrepancies can be seen, the predicted results are generally in good agreement with the measured ones.

Radiation from a circular plate clamped in a duct

In this section, the numerical results of sound radiation from a circular plate clamped in a duct are compared with analytical cal ones, which obtained based on Kirchhoff's thin-plate theory. Figure 7 shows the configuration considered here. The circular plate is assumed to be concrete which has same material parameters as described in the preceding section except for damping parameters: All damping terms are neglected here. The radius is 1500 mm and the thickness is 150 mm. In the FDTD calculation, the spatial intervals Δx=Δy=Δz are set to 30 mm and the time interval is determined to 5 μs. The air layers with a depth of 1000 mm at each side of the plate are surrounded by PMLs with a depth of 1920 mm. Parameters for air are assumed to be same as described in the preceding section except for damping ones.

Figure 8 shows an example of the visualized field of displacement and sound pressure at section including the driving point. The displacements in the figure are multiplied by 40000. Figure 9 shows the numerical and analytical results of impedance level at the driving point. In this figure, eigenfrequencies *in vacuo* obtained based on Mindlin's thick-plate theory are also shown. Discrepancies between eigenfrequencies of analytical results of the thin-plate theory and those of the thick-plate theory can be seen especially at high frequencies because the plate considered here is rather thick. In addition, the discrepancies can be caused by the effect of acoustic load. The numerical results also indicate the slight differences in eigenfrequency with the thick-plate theory. Therefore, to investigate the accuracy of the FDTD method itself, the circular plate *in vacuo* should be calculated. Figure 10 shows the numerical results of impedance level of the circular plate with free boundary conditions. In this case, the eigenfrequencies predicted by the FDTD method well correspond with those of the thick-plate theory.

Radiation from a wooden block

In this section, the numerical and measured data of sound radiation from a wooden block, which is considered as an anisotropic medium, is investigated. Figure 11 shows the configuration considered here and a picture of the experiment is shown in Fig. 12. To minimize the effects of support condition, the wooden block was suspended from the ceiling of the anechoic room and excited by an impulse hammer. In this case, it is sure that the block moves immediately after the excitation and, therefore, the condition of small deformation is not satisfied at quite low frequencies. Two acceleration pickups are located at the excitation-side surface of the block (V. R. 1 and 2) and a microphone is located at 300 mm away

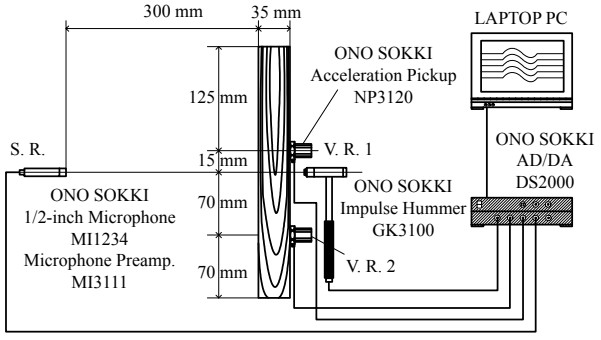

Figure 11. Schematic of the experimental apparatus.

Figure 12. Picture of the experimental apparatus.

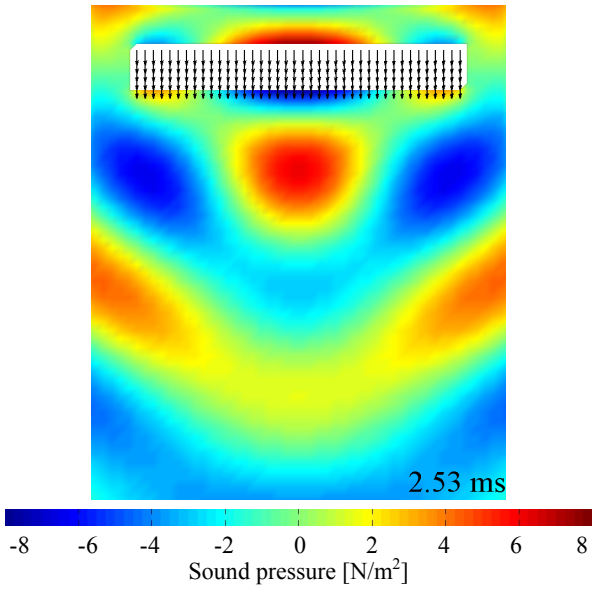

Figure 13. Distribution of displacements and sound pressures.

from the centre of the block (S. R.). Velocities in the normal direction are calculated by integrating measured acceleration values through a high-pass filter with cutoff frequency of 62.5 Hz and sound pressures are measured at a sampling frequency of 44100 Hz. The block is HINOKI cypress with dimensions of 280 × 70 × 35 mm. However, commonly-used material parameter for HINOKI cypress could not be found and there can be also considerable individual variability. Hence the material parameters such as Young's moduli, Shear moduli, Poisson's ratios, and coefficients for damping were identified by use of the measured data. The identification was started with the commonly-used parameters of Picea jezoensis [23] and was performed by trial and error. The identified material parameters are as follows: E_L=1.43 × 10^{10} N/m^2, E_T=4.5 × 10^8 N/m^2, E_R=1.25 × 10^9 N/m^2, G_{LT}=7.0 × 10^8 N/m^2, G_{TR}=6.2 × 10^7 N/m^2, G_{RL}=8.0 × 10^8 N/m^2, υ_{LT}=0.6, υ_{TR}=0.234, υ_{RT}=0.035. The subscripts L, T, and R mean the fibrous direction, tangential direction, and radial direction, respectively. Viscosity coefficients are assumed to be proportional to the initial stiffness and the assumed loss factor is 0.05, and natural angular frequency is set at 2π × 2000 rad/s. constants ζ_d is set as ζ_x=ζ_y=ζ_z=1.17 × 10^5 Ns/m^4. Parameters for air are assumed to be same as described in the preceding section of floor impact noise. Only the density was measured instead and the value is 467 kg/m^3. Allowing for these conditions and the stability condition, the spatial intervals Δx=Δy=Δz are set to 7 mm and the time interval is determined to 0.16 μs.

Figure 13 shows an example of the visualized field of displacement and sound pressure at section including the driving point. The displacements in the figure are multiplied by 20.

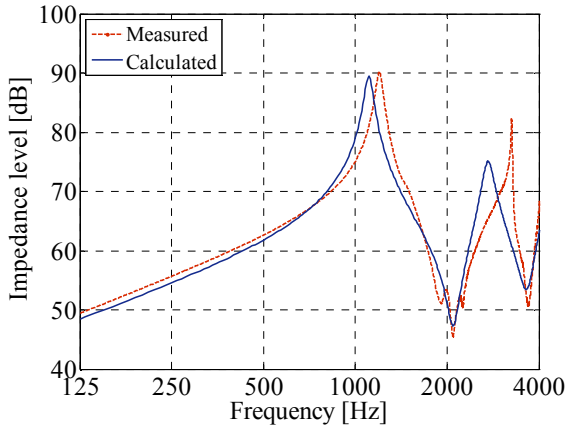

Figure 14. Measured and calculated data at V. R. 1.

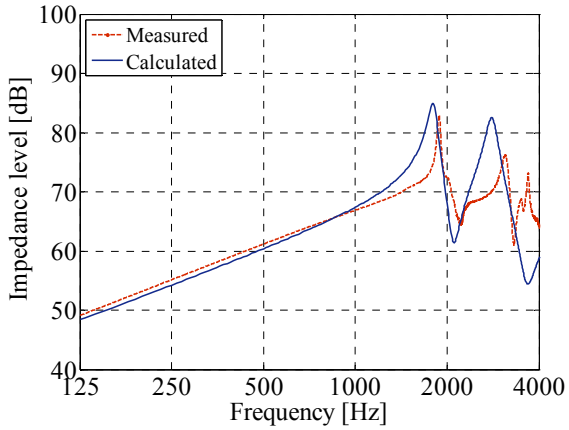

Figure 15. Measured and calculated data at V. R. 2.

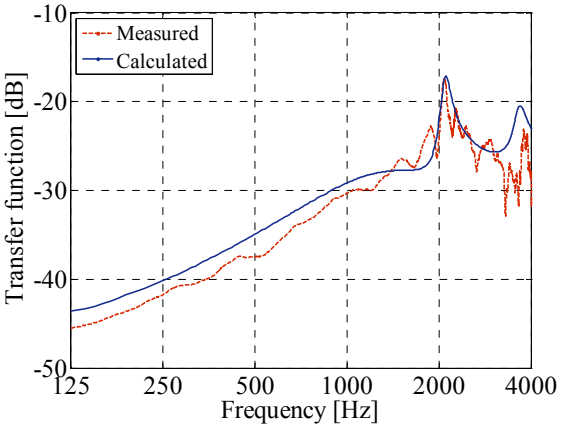

Figure 16. Measured and calculated data at S. R..

Figures 14 and 15 show the calculated and measured results of the impedance levels at V. R. 1 and 2. Figure 16 shows the calculated and measured results of the transfer functions at S. R.. In all of these figures, the slight discrepancies can be seen at low frequencies, which would be caused by additional masses of the acceleration pickups: While the mass of the wooden block is 340 g, that of each pickup is 20 g. Therefore the measured data of impedance tends to be higher than the calculated data and the measured data of transfer function tends to be lower than the calculated data. As seen in Fig. 14, although some differences between the antiresonance frequencies can be observed, the calculated resonance frequencies are in good agreement with the measured ones. As for V. R. 2, both of the calculated antiresonance and resonance fre-

quencies do not correspond with the measured ones well. This would be due to the assumption of orthotropy and further investigations should be needed. In Fig. 16, the measured data has some peaks and dips, which can not be seen in the calculated data. These peaks and dips would be caused by the sound radiation from the moving block.

CONCLUSION

The finite-difference time-domain method considering longitudinal and shear waves and two types of damping terms is proposed for a prediction of radiated sound from inhomogeneous anisotropic media. In the method, both solids and fluids are assumed to be governed by a unique set of motion equations and viscoelastic constitutive equations using averaged material parameters. Herein the formulation and some numerical examples are presented. From these investigations, this method can predict both the vibration of a wide range of materials and the radiated sound. Although the method has a weakness of its huge computational load, it is expected that the method would become helpful for vibroacoustic problems by further improvement of computational processing performance.

ACKNOWLEDGMENTS

This study was partially supported by Program for Improvement of Research Environment for Young Researchers from Special Coordination Funds for Promoting Science and Technology (SCF) commissioned by the Ministry of Education, Culture, Sports, Science and Technology (MEXT) of Japan. This study in part was also supported by the Ministry of Education, Science, Sports and Culture, Grant-in-Aid for Young Scientists (B), 22760440, 2010. We would like to thank Mr. Manabu Tanaka and Mr. Tsuyoshi Murakami for helping with the measurements of floor impact noise at the General Building Research Corporation of Japan. We would like to thank Mr. Hideo Miyazaki for providing a wooden block and helpful discussions at the YAMAHA Corporation. We would also like to thank Mr. Yoshihide Shiba and Mrs. Ami Tanaka for giving many informative suggestions at the Nikken Sekkei Ltd..

REFERENCES

1 K. S. Yee, “Numerical solution of initial boundary value problems involving Maxwell's equations in isotropic media“ *IEEE Trans. Antennas Propagat.* **14**, 302--307 (1966).
2 A. Taflove and S. C. Hagness, *Computational Electrodynamics the Finite-Difference Time-Domain method 3rd edition* (Artech House Publishers, Boston, 2005).
3 T. Uno, *Finite Difference Time Domain Method for Electromagnetic Field and Antennas* (Corona Publishing Co., Ltd., Tokyo, 1998) (in Japanese).
4 M. Sato, *Introduction to the Application of the Finite-Difference Time-Domain Method to Elastic Waves and Vibrations* (Morikita Publishing Co., Ltd., Tokyo, 2003) (in Japanese).
5 M. Sato, “Fundamental Investigation of Shear and Surface Elastic Waves in Soft Biological Tissues by Numerical Simulation“ *Jpn. J. Appl. Phys.* **34** Part 1 (5B), 2808--2811 (1995).
6 F. Iijima, T. Tsuchiya and N. Endoh, “Analysis of Characteristics of Underwater Sound Propagation in the Ocean by a Finite Difference Time Domain Method“ *Jpn. J. Appl. Phys.* **39** Part 1 (5B), 3200--3204 (2000).
7 J. LoVetri, D. Mardare and G. Soulodre, “Modeling of the seat dip effect using the finite-difference time-domain method“ *J. Acoust. Soc. Am.* **100**, 2204--2212 (1996).
8 T. Yokota, S. Sakamoto and H. Tachibana, “Visualization of sound propagation and scattering in rooms“ *Acoust. Sci. Tech.* **23**, 40--46 (2002).
9 Y. Yasuda, A. Ushiyama, S. Sakamoto and H. Tachibana, “Experimental and numerical studies on reverberation characteristics in a rectangular room with unevenly distributed absorbers“ *Acoust. Sci. Tech.* **27**, 366--374 (2006).
10 S. Sakamoto, T. Seimiya and H. Tachibana, “Visualization of sound reflection and diffraction using finite difference time domain method“ *Acoust. Sci. Tech.* **23**, 34--39 (2002).
11 T. Saiki, T. Yokota, S. Sakamoto and H. Tachibana, “Study on sound insulation of double-pane window by FDTD method“ *Proc. Spring Meeting Acoust. Soc. Jpn.*, 873--874 (2002) (in Japanese).
12 M. Toyoda and D. Takahashi, “Prediction for architectural structure-borne sound by the finite-difference time-domain method“ *Acoust. Sci. Tech.* **30**, 265--276 (2009).
13 J. A. G. Temple, “Modelling the propagation and scattering of elastic waves in inhomogeneous anisotropic media“ *J. Phys. D: Appl. Phys.* **21**, 859--874 (1988).
14 H. Hatano, I. Yoshijima, M. Fujiwara, T. Shin-nashi and C. Yamashita, “Finite-difference simulation of ultrasonic testing for acoustically anisotropic rolled steel“ *J. Acoust. Soc. Jpn.* **63**, 139--147 (2007) (in Japanese).
15 H. Suzuki, A. Omoto and K. Fujiwara, “Treatment of boundary conditions by finite difference time domain method“ *Acoust. Sci. Tech.* **28**, 16--26 (2007).
16 J. P. Berenger, “A perfectly matched layer for the absorption of electromagnetic waves“ J. Comp. Phys. 114, 185--200 (1994).
17 W. C. Chew and Q. H. Liu, “Perfectly matched layers for elastodynamics: a new absorbing boundary condition“ *J. Comp. Acoust.* **4**, 341--359 (1996).
18 H. W. Chang and C. J. Randall, “Finite--difference time--domain modeling of elastic wave propagation in the cylindrical coordinate system“ *Proc. IEEE Ultrasonics Symp.*, 397--402 (1988).
19 C. J. Randall, D. J. Scheibner and P. T. Wu, “Multipole borehole acoustic waveforms: Synthetic logs with beds and borehole washouts“ *Geophysics* **56**, 1757--1769 (1991).
20 R. W. Graves, “Simulating seismic wave propagation in 3D elastic media using staggered-grid finite differences“ *Bull. Seis. Soc. Am.* **86**, 1091--1106 (1996).
21 Q. H. Liu, E. Schoen, F. Daube, C. Randall, H. L. Liu and P. Lee, “A three-dimensional finite difference simulation of sonic logging“ *J. Acoust. Soc. Am.* **100**, 72--79 (1996).
22 R. Vossen, J. O. A. Robertsson and C. H. Chapman, “Finite-difference modeling of wave propagation in a fluid-solid configuration“ *Geophysics* **67**, 618--624 (2002).
23 Forestry and Forest Products Research Institute, *Handbook of wood industry 4th edition* (Maruzen, Tokyo, 2004) (in Japanese).